RSC Advances




ROYAL SOCIETY OF CHEMISTRY

www.rsc.org/advances

Journal Name

ARTICLE

Received 00th January 20xx,
Accepted 00th January 20xx
DOI: 10.1039/x0xx00000x
www.rsc.org/

# Colloidal silver nanoparticles: an effective nano-filler material to prevent fungal proliferation in bamboo

O. Pandoli,[a] R. D. S. Martins,[a] E. C. Romani,[b] S. Paciornik,[c] M. H. D. P. Maurício,[c] H. D. L. Alves,[d] F. V. Pereira-Meirelles,[a] E. L. Luz,[a] S. M. L. Koller,[a] H. Valiente[c] and K. Ghavami[e]

*Silver nanoparticles (Ag-NPs) have attracted attention as a promising nano-filler material for reinforcement and anti-bacterial effect in polymers and composites. In this work bamboo samples, Dendrocalamus Giganteus Munro, were impregnated using a colloidal solution of homemade Ag-NPs with the goal of improving its resistance to the attacks by fungi. X-ray microtomography (μCT) was performed to investigate the 3D distribution of the Ag-NPs within the biological matrix. 3D image reconstruction showed silver clusters distributed within the parenchymatic tissue. Quantitative information of the Ag-NPs agglomerate population was computed. Ag-NPs were characterized by UV-VIS, SERS, ICP-MS, TSEM, DLS and zeta potential analysis. The antimicrobial activity of homemade and commercial citrate-capped silver nanoparticles was evaluated against the Aspergillus niger fungus. Homemade nanoparticles (NP-01), presenting the smallest diameter (14.3±3.6 nm), and the highest particle concentration ($1.25x10^{11}$ particle $mL^{-1}$) were able to inhibit 53% of Aspergillus niger growth in a concentration of 2.00 mg $L^{-1}$. Both engineered biocomposite material and untreated specimens were exposed to air and humidity. After five months the treated samples were free of fungal colonies, while colonization by the fungal hyphae were present on untreated bamboo specimens.*

## Introduction

The use of bamboo has been investigated in lieu of raw materials in engineering, biomass production, power plant, furniture, textiles, paper, composite panels, decoration materials, building material and handcrafts.(1,2) Nevertheless, the application of natural bamboo has been restricted due to its degradation, which is affected by microbiological activity.(3–5) In this regard nanotechnology is focused on the use of silver nanoparticles against insects, bacteria and fungi, affecting the metabolism of these microorganisms, for industrial and biomedical applications.(6)

Among all the inorganic nanoparticles (NPs) based on gold (Au), silver (Ag), copper (Cu), zinc (Zn) and titanium (Ti), Ag-NPs are one of the most used engineered nanostructured materials for industrial applications and academic research. Inorganic nanoparticles, defined as nanofillers: *"are reinforcement particles smaller than 100 nm in size which are usually blended with resins to create nanofilled resin composites. Incorporation of nanofillers into resin composites enables mechanical strengthening and excellent surface polishing*".(7) Relatively easy to synthesize and characterize, Ag-NPs have good chemical stability when capped with proper organic stabilizer, high biocompatibility with human and plants, easy commercial availability and large atomic weight if compared to bamboo matrix, leading to significant image contrast in microtomography studies. Antifungal effect of silver nanoparticle (Ag-NPs) against plant pathogenic fungi has already been studied with success.(8,9) Ag-NPs can act as well as potential antimicrobial agents which mechanism inhibition of cell growth by silver ions ($Ag^+$) has been established.(10) Particle size, shape, type of ligand or stabilizer can influence its bactericidal properties.(11,12) There are already several applications in food packaging, food safety and as wound treatment agents.(13–15) Successful treatment of natural fibers with silver nanoparticles as antifungal protector, has also been reported.(16,17) Recently, a review shows a large number of nanomaterials used for dental care and dentistry which may improve mechanical reinforcement, aesthetic aspects, beyond inducing antimicrobial and therapeutic effects. Among them, Ag-NPs are already successfully used for dental care. (7,18) In the plant nanobiotechnology field, silver nanoparticles are used in plant tissues instead of classical antibiotics and chemotherapeutic agents to avoid phytotoxicity, retard plant tissue growth or risk of resistance to bacteria in case of extended exposure to conventional drugs.(19) In nanoagriculture, engineered nanomaterials are used to increase the yield of plant for food and fuel.(20)

Hamed *et al*., reported an in-vitro study about the biodegradation of wood by the *Aspergillus niger* fungus.(21) The work focus was to illustrate the morphological and structural wood decay induced by fungi. The concern was the lack of a conservation method or lifting procedure to preserve historically wooden artefacts.

The incorporation of silver, copper and zinc oxide nanoparticles into paints have been studied to inhibit molds growth in indoor environments and therefore to prevent air contamination. The best results were obtained incorporating silver nanoparticles with the smallest size (10 nm).(22) Nowadays, two patents involving silver NPs as biocidal agents are already deposited: Horner *et al.,* reported a practical application using nanosilver as an antimicrobial agent in

[a]Chemistry Department, PUC-Rio, Rio de Janeiro, Brazil
[b]Physic Department, PUC-Rio, Rio de Janeiro, Brazil
[c]Chemical and Materials Eng. Department, PUC-Rio, Rio de Janeiro, Brazil
[d]Applied Physics and Thermodynamics Department, UERJ, Rio de Janeiro, Brazil
[e]Civil Eng. Department, PUC-Rio, Rio de Janeiro, Brazil

Electronic Supplementary Information (ESI) available: TSEM image of Ag-NPs. See DOI: 10.1039/x0xx00000x

building material for roofing, insulation, cladding, wall lining;(23) Kwon *et al.,* developed an antibacterial paint containing silver nanoparticles.(24) A cheaper alternative to silver NPs is based on copper oxide nanoparticles. Meghana and. Usman *et al.,* reported its potential antimicrobial activity against bacteria. (25,26) In this early stage, no works are presented against fungus, or its potential hazard due to prolonged exposure of human beings and environment [3,5]

Bamboo is considered an important non-conventional building material for low income housing and sustainable urban architecture, but its response to microbiological activity is not yet established for biological decay.(27) It is a giant grass, and not a tree as commonly believed, belonging to the *Bambusoideae* family and found in large quantities in Asia, Africa and South America. Their culms are generally a cylinder shell, divided by transversal diaphragms at the nodes. The structure of bamboos is a composite material, mainly composed of multi-functional fibers of cellulose (55%), lignin (25%) and hemicellulose (20%).(28) Aligned cellulose fibers immersed in ligneous matrix are distributed anisotropically in a radial direction from the inner to outer section of the culm.(29) This structural composition, named sclerenchyma is responsible for bamboo's mechanical strength (30,31) and, at the same time, it supports the vascular bundles system to feed all the living cells of the parenchymal tissue. Due to its chemical, physical and mechanical properties, bamboo presents high versatility and viability to replace wood and steel.(32) In addition, cellulose bamboo pulp can act as reinforcement in composites,(33) and in concrete to replace asbestos and glass fibers.(34)

Within parenchymal tissue of the biological matrix there are starch granules and water, which are an energy source for the growth of microorganisms, which are prone to their attacks, especially by fungi and insects. In order to passive the bamboo from biological degradation, different methodologies have been explored, such as, immersion in boiling water, injection of water with positive pressure (Boucherie method) (35), and impregnation with polymeric resin.(36) To reduce the degradation of bamboo and to preserve the external aspect as well as all the mechanical properties, a treatment with antifungal chemical compounds, such as borax-boric acid mixture, ammonium compound or copper-chrome-arsenic, have been investigated, but not with total success. (4,37) Bamboo pulp(38) and bamboo rayon fabric(17) were grafted with silver and copper nanoparticles, respectively. Jingpeng Li *et al.,* have successfully deposited different nanostructured materials onto external bamboo surface creating: 1) a superhydrophobic bamboo timber based with $TiO_2$ anatase film for a self-cleaning and acid rain protection,(39,40) 2) Ag-NPs external deposition to construct a durable robust superhydrophobic surface with high conductivity,(41) 3) ZnO nanocoating surface with improved mould-resistance.(42,43)

In this work, for the first time, we propose to fill the bamboo matrix with silver colloids as nanofiller agents to verify its effectiveness against microbiological attacks, especially fungi.(44) Fungi is a kingdom containing a lot of micro-organisms divided into phylum, class, order, family, genus and species.(45) Many species are able to attack wood and bamboo, including the *Aspergillus* species.(21,46) *Aspergillus niger* is one of the most important species from this genus, for both industry and the environment.(47,48) These cells are able to produce lots of metabolites and enzymes involved in cellulose, hemicellulose and lignin degradation.(49) *Aspergillus niger* is easily cultivated, its morphology and metabolism are well understood and its cell growth is faster than for other fungus.(47) To save time and to avoid possible degradation of silver NPs in the culture medium during extended biological experiment, in this work, we decided to use *Aspergillus niger.* For all these mentioned reasons, we preferred to work with this fungi as a non-pathogenic fungus widely distributed in nature and to avoid opportunistic human pathogenic fungus.

The impregnation with an aqueous colloidal solution of Ag-NPs can take advantage from the hydrophilic surface properties of bamboo fibers.(50) In this regard to enhance the dispersion of the Ag-NPs the right choice of organic surfactant ligand is critical. X-ray microtomography (µCT) was chosen as the imaging technique to reveal the metal distribution within the bamboo matrix. µCT is a non-destructive technique that relies on the interaction and attenuation of X-rays when passing through a sample.(51,52) This technique is particularly suitable in this case, given the large atomic weight difference between the silver particles and the bamboo matrix, leading to significant image contrast. The technological advancements on X-ray tubes with smaller focal spot sizes and flat panel detectors made resolution at the micron scale possible. The result of µCT is a 3D image of the internal structure of the biocomposite sample, which allows a 3D analysis of parameters that are usually limited to a 2D evaluation.(53). Considering that µCT offers thousands of images and true 3D information, the statistics are far superior to any other available non-destructive technique. The advantages of the technique have been recognized in several areas of expertise such as orthodontics, biology, earth sciences, archaeology, and many others.(54–59)

In this study, the nanofiller agent (Ag-NPs) was used to fill up the biological matrix of bamboo to obtain an engineered biocomposite. The silver deposition into bamboo matrix was analysed by means of µCT and quantitative information of the silver clusters was extracted using digital processing 3D images. Finally, optical microscope observation was performed to confirm the growth inhibition of fungal colonies on bamboo sample.

## Experimental

### Materials and methods

Silver nitrate ($AgNO_3$, >99.9% pure), sodium borohydride ($NaBH_4$, >99% pure), and trisodium citrate ($Na_3$Citrate, >99.0% pure) were purchased from Sigma-aldrich and used as received. Water obtained from a Millipore MilliQ purification system (resistivity ≥ 18.2 MΩ $cm^{-1}$) was used to make all the solutions for the desired reactions. For the synthesis of silver nanoparticles, in flow mode, two syringe pumps (Future Chemistry) and one glass microreactor (Micronit) were used. The syringe pumps are able to inject the solutions of silver precursor and organic ligand into the microchannel device to improve the mixing and the formation of the organic-metal complex in a shorter time when compared with the batch mode. PFA (perfluoroalkoxyalkane) tubes and PEEK connections (polyetheretherketone) (UpChurch) were used to inject the two solutions into the microreactor with 6 µL internal volume. Commercial PELCO Citrate NanoXact™ Silver Nanospheres with diameters about 20 nm (CO-20), 40 nm

(CO-40) and 60 nm (CO-60) purchased from TedPella Inc were also used. The bamboo impregnation experiments were carried out using a four years old *Dendrocalamus giganteus* bamboo culm obtained from FZEA-USP, Pirassununga-SP, Brazil. Microbiological tests were performed with the *Aspergillus niger* fungus strain, grown in liquid Sabouroud, Kasvi (Slabor). The samples were cut with an automatic precision cut-off machine, Miniton from Struers, using a wafering blade made of diamond metal bonded, 3" x 0.006" x ½" (76 x 0.15 mm).

**Synthesis procedures**

Ag-NPs were synthesized employing $NaBH_4$ as reducing agent and $Na_3$Citrate as stabilizer organic ligand. In the first step of organic-metal complex formation, $Na_3$Citrate organic ligand with three carboxylate functional groups was able to coordinate silver ions ($Ag^+$) into the microfluidic device. In the second step, during the chemical reduction of $Ag^+$ to silver metal nanoparticles, $Na_3$Citrate acted as a capping agent, preventing the aggregation of Ag-NPs. The reduction process was conducted in continuous flow reaction, in which $AgNO_3$ solution ($10^{-2}$ mol $L^{-1}$) was mixed with sodium citrate organic ligand ($10^{-2}$ mol $L^{-1}$) in a glass of microreactor system.(60) The two solutions were injected by means of two syringe pumps at a flow rate of 0.25 mL $min^{-1}$. The $Ag^+$: ligand complex flowing out of the microreactor dropped directly into the fresh $NaBH_4$ solutions ($10^{-2}$ mol $L^{-1}$) under vigorous stirring, at room temperature. Colloidal solution NP-01 was used for the antimicrobial tests and impregnation of a bamboo specimen.

**UV-VIS Spectroscopy**

The colloidal suspensions of Ag-NPs were characterized using UV–vis spectrophotometer model Lambda 950 from Perkin Elmer, USA), with a spectral resolution of 1.0 nm and a spectral range between 300–500 nm. For the UV-VIS spectrophotometric analysis, all commercials nanoparticles were diluted with Millipore MilliQ water in the ratio 1:4, with the exception of NP-01, which was diluted in the ratio 1:40.

**RAMAN and surface-enhanced Raman scattering (SERS) spectroscopy**

Raman and SERS spectroscopy were performed using a micro-Raman microscope (HORIBA, model XploRA), at the exciting wavelengths of 638 nm. The laser excitation beam was focused onto the liquid samples with an intensity of 25 $Wmm^{-2}$ by a 10x objective lens. The scans were performed using a fixed acquisition time of 5 s with 20 accumulations, with a range between 550 and 1800 $cm^{-1}$ and a spectral resolution of 4 $cm^{-1}$. Raman spectra of trisodium citrate aqueous solution (1.5 mol $L^{-1}$) was acquired and compared with the SERS spectra of citrate-capped Ag-NPs. In order to observe the SERS of citrate-absorbed Ag-NPs, sequentially, 3 drops of NPs suspensions were deposited on a silicon wafer to induce Ag-NPs aggregations by slow evaporation of the water solvent. Before the aggregation of NPs only background scattering was observed.

**Morphological characterization by TSEM**

For the morphological characterization of Ag-NPs using microscopy, a small drop (2.5 μL) of the nanoparticle solution NP-01 was placed on a carbon grid (holey carbon) and allowed to evaporate completely in the air before analysis. A field emission scanning electron microscope (FEG-SEM) (JEOL, JSM-6701F) operated in the transmission mode (TSEM) at 30 kV with a work distance of 6.0 mm using the bright-field detector was used. A longitudinal section of bamboo vascular bundle was also observed in scanning mode (SEM) at 1 kV with a work distance of 14.7 mm.

In order to obtain the size distribution of silver nanoparticles, an image analysis (IA) routine created in the FIJI/ImageJ program was applied. An intensity threshold was used for segmentation, followed by watershed separation to detect the individual silver nanoparticles. The particles´ major and minor axes were measured, among other morphological attributes. Diameter distributions were inserted in the corresponding TSEM images with a mean value of 14.3±3.6 nm for NP-01, 21.2±3.2 nm for CO-20, 38.9±7.3 nm for CO-40 e 60.3±8.9 nm for CO-60. The results are in good agreement with the technical data sheet of the commercial nanoparticles purchased from TedPella Inc.

**Element Ag detection by ICP-MS**

The quantification of the concentration of colloids Ag-NPs was performed by inductively coupled plasma mass spectrometry (ICP-MS) to confirm the data of commercial nanoparticles (CO-20/40/60) and homemade NP-01. ICP-MS (Perkin Elmer, ELAN Drc II Axial Field Technology) data acquisition was performed using 20 sweeps, in triplicate, and a dwell time of 50 ms. Default values were used for the rest of instrumental parameters. After acid digestion with concentrated $HNO_3$ in hot plate for 10 minutes, the diluted silver ionic solutions were direct injected and compared with the ionic silver standard solutions (5-30 ppm) into the ICP-MS system.

**Size distributions and Zeta potential analysis**

Size distribution by DLS and zeta potential of nanoparticles for the colloid solutions were measured with a Nano-100SZ (Horiba instrument). NP-01 colloid solution was diluted to reach a citrate concentration of $2.0x10^{-3}$ mol $L^{-1}$, as indicated on the technical data sheet for the Ag-NPs commercialized by TedPella Inc. Before the analysis, the solutions were filtered through a 0.20 μm membrane, Cromafil® EXTRA PTFE-20/25. Measurement parameters were as follows: water viscosity medium of 0.894 mPa $s^{-1}$; refractive index dispersion medium of 1.333; detector scattering angle of 90°; temperature of 25 °C; particle refractive index for silver of 0.130-3.200i. For all samples, the count rate was between 500 and 1200 kCps. The polydispersity index (PDI) for the colloids silver nanoparticles was smaller than 0.58.

**Bamboo impregnation**

A 5x5x5 mm cubic section of *Dendrocalamus Giganteus Munro* bamboo was placed into a test tube with 0.50 mL of citrate-capped colloidal solution of silver nanoparticles (NP-01) for 2 hours. It was submitted to five impregnation cycles through a vacuum system. After each cycle, a fresh NP-01 solution was used. Then the impregnated bamboo specimen was analysed with X-ray microtomography.

**X-Ray Microtomography (µCT)**

A Zeiss Xradia Versa 510 microtomograph was employed. This system consists of an X-ray microfocus source, with up to 160 kV voltage and 10 W power and a detection system in which two-stage magnification scheme is used: i. geometric magnification as with conventional µCT, ii. a set of optical lens with scintillators converts X-rays to visible light, which is then optically magnified. Achievable true spatial resolution reaches 0.7 µm. The bamboo samples, before and after Ag-NPs impregnation, were scanned using the configurations presented in Table 1. A 3D digital video rendered from the µCT reconstructed images was used to visualize the different biological structures and the volumetric metal deposition within the engineered biocomposite material. This video is available through the following link https://www.youtube.com/watch?v=gbbyCVz3Pw0g.(61)

Table 1 X-Ray Microtomography (µCT) parameters

| | Sample 1 Pure bamboo | Sample 2 Bamboo /Ag-NPs |
|---|---|---|
| Voltage (kV) | 80 | 40 |
| Power (W) | 7 | 3 |
| Pixel size (µm) | 4 | 3.43 |
| Exposure Time (s) | 0.2 | 1 |
| Number of Projections | 1600 | 1600 |

**Image processing and analysis of µCT images**

The µCT images of the impregnated bamboo specimen were processed and analyzed using FIJI/ImageJ free software.(62,63) The volume distribution and statistical information of Ag-NPs aggregates population in the bamboo matrix were obtained.

**Microbiological Tests**

The antimicrobial activity of Ag-NPs was evaluated. For this purpose, *Aspergillus niger* was cultivated in Sabouroud liquid medium at 29°C and 160 rpm in the presence and absence of Ag-NPs in the test tubes.(44) A volume of 1 mL of culture medium without Ag-NPs was used as a positive control for cell growth. Commercial and homemade colloidal solutions of Ag-NPs with original concentration as shown in table 4 where introduced in 1 mL inoculated culture media with a final concentration of 2.00 mg $L^{-1}$ of each type of Ag-NPs. Microbial growth was followed during 24 and 48 hours. After 48h, the tubes were vacuum filtered, and the pellets were dried in an oven at 60°C. At different times, they were weighed with an analytical balance until constant dry weight. All the experiments were conducted in triplicate.

## Results and discussion

**Ag-NPs characterization.** The Localized Surface Plasmon Resonance (LSPR) band of a diluted silver colloidal solution is presented in Figure 1. The peak absorption of the LSPR band is centred at 393.1 nm for the homemade silver nanoparticles, NP-01. The plot also shows the spectra for commercial nanoparticles with 20 nm, 40 nm and 60 nm, with peak absorptions at 398.5 nm, 409.0 nm and 431.8 nm, respectively. According to the theory of surface plasmon resonance, the LSPR band of colloidal solutions is highly dependent on the diameter of silver nanoparticles.(64) Thus,

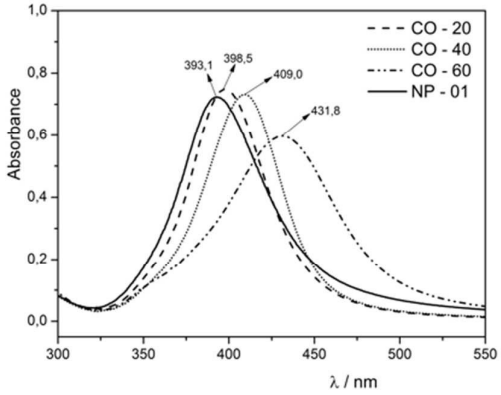


Fig. 1 UV-VIS spectra of diluted colloidal solutions of citrate capped Ag-NPs. Homemade (NP-01) and commercial colloidal solutions (CO-20, CO-40 and CO-60).

the smallest wavelength for NP-01 indicates a colloidal solution contains smaller particles than the commercial ones.

The Raman spectra of the trisodium citrate is reported in Figure 2 and its scattering bands summarized in Table 2. The most intense single band Raman scattering is attributed to the carboxylate symmetric stretching band, $\upsilon_s$(COO), at 1406 $cm^{-1}$. This band is broadened and shifted, from 1375 to 1383 $cm^{-1}$, in the SERS spectra of citrate absorbed on the surface of the commercial Ag-NPs (CO-20/40/60) (Figure 3). This is possibly due to the interaction between the carboxylate groups and the silver metal surface. The broad band of the carboxylate symmetric stretching band indicates that the interactions with the metal surface are not equivalent, supposing that one of them might point out of the surface as confirmed by the zeta-potential measurements with a value up to -40 mV.(65)

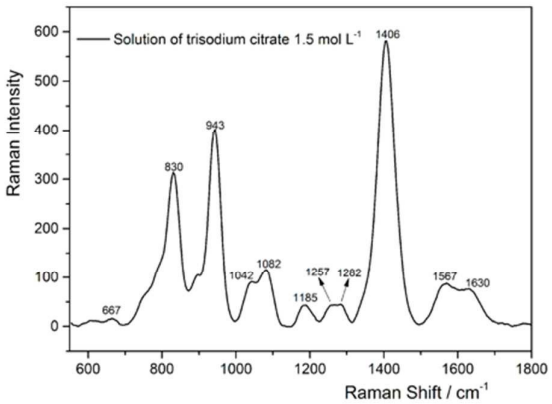


Fig. 2 Raman spectra of aqueous solution of trisodium citrate (1.5 mol $L^{-1}$) by excitation at 638 nm.

Table 2 Raman frequencies and band assignments for the aqueous solution of trisodium citrate (1.5 mol$L^{-1}$).(66–68)

| Frequency ($cm^{-1}$) | Assignment | Frequency ($cm^{-1}$) | Assignment |
|---|---|---|---|
| 1567-1630 | $\upsilon_a$(COO) | 943 | υ (C-COO) |
| 1406 | $\upsilon_s$(COO) | 830 | υ (C-C) |
| 1257-1282 | δ (COO) | 667 | $\delta_{out\text{-}plane}$(COO) |
| 1042-1082 | υ (C-OH) | | |

The weak double band Raman scattering at 1567–1630 $cm^{-1}$ is attributed to the carboxylate asymmetric stretching band, $\upsilon_a$(COO), of pure citrate. These broadened bands are thin and centred at 1602 $cm^{-1}$ in the SERS spectra of the commercial Ag-NPs. This enhancement of the asymmetric vibration can corroborate the hypothesis of interactions between the carboxylate groups and the metal nanoparticle. An isolated SERS band, at 1721 $cm^{-1}$ for citrate-reduced silver colloids, was observed for the first time by Muoro *et al.*(68) It was attributed to the presence of decomposition products of citrate, such as, acetone dicarboxylic acid and acetoacetic acid. All these compounds with similar carboxylate groups can justify the broadening of the $\upsilon_s$(COO) from 1314 to 1467 $cm^{-1}$.

For the commercial NPs we did not obtain disclosed information about the chemical preparation. For this reason it is difficult to justify and compare SERS spectra of homemade NPs with the commercial ones. Our homemade NPs are borohydride-reduced colloids what might justify the absence of the isolated SERS band at 1721 $cm^{-1}$. In Figure 3, the SERS of homemade NPs confirms the presence of carboxylate symmetric stretching band, $\upsilon_s$(COO), centred at 1393 $cm^{-1}$, but the carboxylate asymmetric stretching thin band, $\upsilon_a$(COO), is broadened, weak and shifted to 1551 $cm^{-1}$. The bending vibration of carboxylate group, δ(COO), in the Raman spectra of pure citrate, appears as double bands from 1257 to 1282 $cm^{-1}$. SERS δ(COO) bands appeared at 1279 and 1296 $cm^{-1}$, respectively, for citrate absorbed on CO-60/40/20 e NP-01. All other SERS bands, summarized in tables 3 e 4, overlap with a small red shift that might be due to the different chemical nature of borohydride-reduced colloids suspensions (NP-01).(66,67)

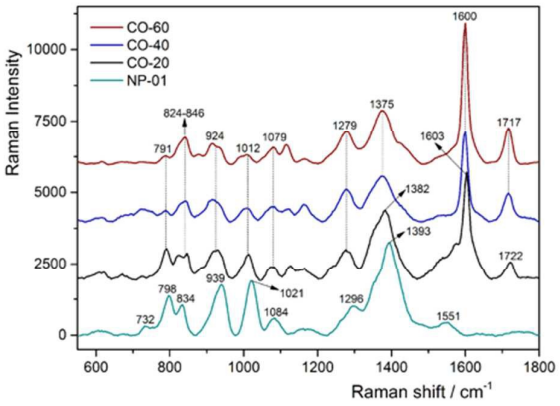


Fig. 3 SERS spectra of citrate absorbed to nanoparticle surface obtained by excitation at 638 nm for CO-60 (red line), CO-40 (blue line), CO-20 (black line) e NP-01 (green line).

Table 3 SERS frequencies and band assignments for citrate absorbed on the metallic surface of commercial Ag-NPs aggregated from 3 drops of suspensions of CO-60, CO-40 e CO-20 on silicon wafer.(66–68)

| Frequency [$cm^{-1}$] | Assignment | Frequency [$cm^{-1}$] | Assignment |
|---|---|---|---|
| 1600-1603 | $\upsilon_a$(COO) | 1112 | υ (C-O) |
| 1375-1382 | $\upsilon_s$(COO) | 924 | υ (C-COO) |
| 1279 | δ (COO) | 824-846 | υ (C-C) |
| 1079 | υ (C-OH) | 791 | $\delta_{out\text{-}plane}$(COO) |

Table 4 SERS frequencies and band assignments for citrate absorbed at the surface of homemade Ag-NPs (NP-01) aggregated from 3 drops of suspension on silicon wafer.(66–68)

| Frequency [$cm^{-1}$] | Assignment | Frequency [$cm^{-1}$] | Assignment |
|---|---|---|---|
| 1551very weak | $\upsilon_a$(COO) | 1121 | υ (C-O) |
| 1393 | $\upsilon_s$(COO) | 939 | υ (C-COO) |
| 1296 | δ (COO) | 834 | υ (C-C) |
| 1084 | υ (C-OH) | 798 | $\delta_{out\text{-}plane}$(COO) |

Table 5 Quantification of element (Ag) mass concentration and particles concentration for the colloids suspensions by direct injection of acid digested NPs solutions into ICP-MS.

| Sample | Mass Concentration (Ag) [mg $L^{-1}$] | Mass Concentration (Ag) in 1mL media [mg $L^{-1}$] | Diameter from TSEM image [nm] | Particles Concentration in 1 mL media [particles $mL^{-1}$] |
|---|---|---|---|---|
| NP–01 | 229.00±0.31 | 2.00 | 14.3±3.6 | $1.25x10^{11}$ |
| CO–20 | 16.66±0,09 | 2.00 | 21.2±3.2 | $3.82x10^{10}$ |
| CO–40 | 21.31±0.10 | 2.00 | 38.9±7.3 | $6.19x10^{9}$ |
| CO–60 | 21.28±0.17 | 2.00 | 60.3±8.9 | $1.66x10^{9}$ |

ICP-MS analysis results of element (Ag) mass concentration are summarized in Table 5. The results for the commercial NPs from 17 to 22 mg $L^{-1}$ showed a good agreement with the technical data sheet of the commercial nanoparticles. Aliquots of the mother solutions were injected in 1 mL fungus medium with an equal final concentration of 2.00 mg $L^{-1}$. From the element (Ag) mass concentration and the size diameter distribution from TSEM images (Figure S1) we estimated the particle concentration of each colloid used for the microbiological tests. Homemade nanoparticles (NP-01) presenting the smallest diameter of 14.3±3.6 nm show a particle concentration ($1.25x10^{11}$ particles $mL^{-1}$) 3.3 fold higher with respect to the smallest commercial nanoparticle CO-20 ($3.82x10^{10}$ particles $mL^{-1}$). How will be shown in the microbiological test, the best biocidal activity of NP-01 is due to both reasons: the smaller size diameter, as reported previously,(69,70) and the higher number of NPs able to act against the fungus.

**Colloid Stability.** Homemade NPs (NP-01) and commercial NPs (CO-20/40/60) were stored in the same conditions: at +5˚C and protected from the light. The DLS and zeta potential experiments were done with 5 month aged silver NPs. DLS size distribution shown by particle number is plotted in Figure 4 and summarized in Table 6. Hydrodynamic diameter of all colloids suspensions confirms the size distribution obtained by TSEM analysis distribution (Figure S1). As well established in the literature,(65) the hydrodynamic diameter of NPs does not depend only on the metal core, but also on the organic ligand absorbed on the surface of the nanoparticle and the thickness of the electrical double layer (solvation shell). For these reasons the size distribution measured with DLS is higher in comparison to the TSEM analysis distribution.

Aged NPs with zeta potential of about –40mV, confirms the stability of the NPs suspensions with pendant negative carboxylate groups of citrate absorbed on metal Ag-NPs.(65) NPs negatively charged by citrate ions are stabilized by electrostatic repulsions. Also, SERS spectra of aged NPs were acquired to confirm the presence of citrate ions absorbed on their surface (Figure 3). We would like to highlight that all the biological and impregnation experiments were done with fresh synthetized NPs.

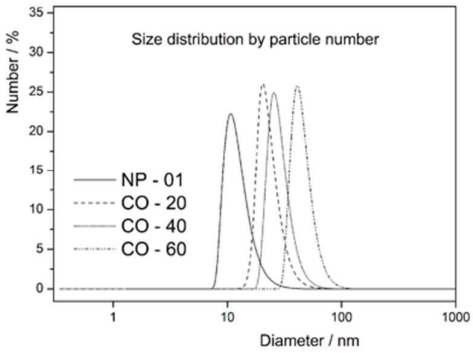


Fig 4. DLS size distribution shown by particle number for 5 months aged Ag-NPs colloids: NP-01 (17.2 nm), CO-20 (22.7 nm), CO-40 (44.7 nm) e CO-60 (62.4 nm).

Table 6 Summary results of size distribution of hydrodynamic radius and Zeta-potential for 5 months aged Ag-NPs colloids.

| Sample | Particle Surface Aqueous $Na_3Citrate$ [mol $L^{-1}$] | Hydrodynamic diameter (Z-average) [nm] | PDI | Zeta potential [mV] |
|---|---|---|---|---|
| NP–01 | $2.0x10^{-3}$ | 17.2 | 0.553 | -41.4 |
| CO–20 | $2.0x10^{-3}$ * | 22.7 | 0.587 | -40.5 |
| CO–40 | $2.0x10^{-3}$ * | 44.7 | 0.268 | -43.3 |
| CO–60 | $2.0x10^{-3}$ * | 62.4 | 0.296 | -49.9 |

*data from the technical data sheet of TedPella Inc.*

**Microtomography study.** Three dimensional (3D) µCT images of pure bamboo structures are presented in Figure 5. The light grey colour shows the complex vascular bundles of bamboo with two large circular metaxylem vessels (100µm), phloem and protoxylem wrapped or capped by fibers of sclerenchyma tissue (lignificated vegetable cells). The parenchyma shown in dark grey colour represents the living cells of the bamboo matrix. The parenchyma cells are vertically elongated in rectangular or shorter cube-like shapes, and alternate themself along the culm. The vascular bundles system varies along the bamboo culm length in size, distribution and shape. Meanwhile the tissue arrangements of the vascular bundles are strictly longitudinally oriented, as pillars.(28)

In Figures 6 and 7, 2D and 3D µCT images present bamboo samples after Ag-NPs treatment with 5 cycles of impregnation. The images in Figure 6 show a transversal (XY) and two longitudinal sections (YZ and XZ) of the biocomposite bamboo in which Ag-NPs aggregates are highlighted with red squares. It can be seen that the deposition was concentrated in the parenchyma only, leaving the metaxylem vessels free of Ag-NPs. The random deposition of the bright metal within the living cells of the bamboo matrix is evident in all represented sections. Moreover, the zoomed-in images reveal that metal deposits are vertically elongated in rectangular or shorter cube-like shapes, similar to the shape of the plant cells. In Figure 7A-B, 3D µCT images, with front and lateral projections and pseudo colours, allow to identify silver aggregates inside the bamboo sample. In this case, red and yellow represent the bamboo matrix, and silver aggregates, respectively. In Figure 7C-D the opacity of the bamboo parenchyma was reduced to highlight the silver

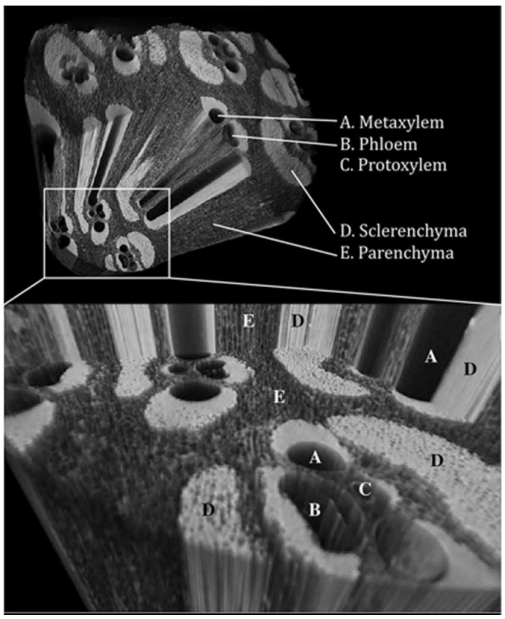


Fig. 5 3D µCT image of pure bamboo specimen shows the complexity of vascular bundles constituted by: (A)metaxylem vessels (100µm); (B)phloem; (C)protoxylem; (D)sclerenchyma fibers and (E)parenchyma tissue.

aggregates within the whole bamboo volume.

The video available online shows the different physical parts of the biocomposite engineered material. One frame of the video is shown in Figure 8. The orange colour represents the sclerenchyma and parenchyma tissues; purple represents the metaxylem, phloem and protoxylem vessels; finally, yellow represents the silver aggregates in the parenchyma matrix. Since µCT cannot show individual nanoparticles due to the limitation in the spatial resolution of this technique, this analysis focused on the study of the agglomerates deposited inside the bamboo matrix.

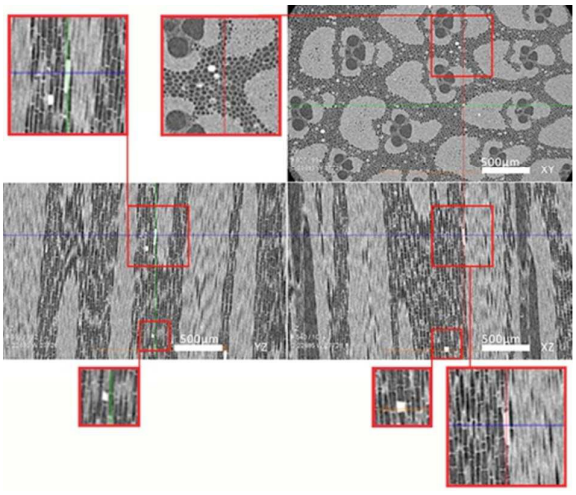


Fig. 6 2D µCT images of bamboo after five impregnation cycles with citrate-capped Ag-NPs. In the transversal (top image) and longitudinal (bottom image) sections, red squares highlight silver aggregates in the parenchyma matrix of bamboo.

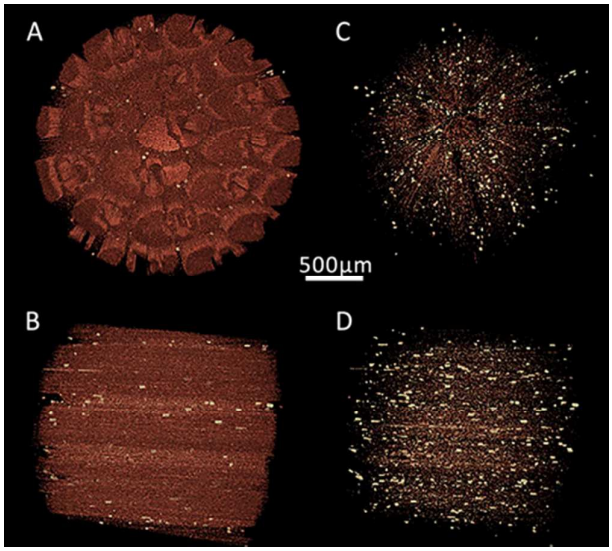


Fig. 7 3D µCT images of bamboo after five impregnation cycles with citrate-capped Ag-NPs. Red and yellow colors represent, respectively, the bamboo matrix and silver aggregates. A-B and C-D are front and lateral side projections.

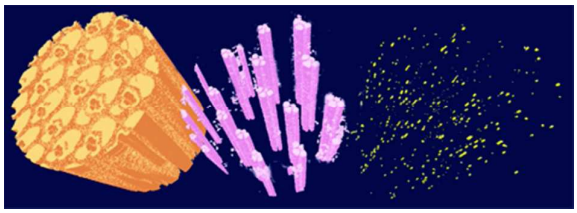

Fig. 8 One frame picture of the on-line video showing different physical parts of the biocomposite engineered material: sclerenchyma and parenchyma tissues (orange); metaxylem, phloem and protoxylem vessels (purple) and silver aggregates (yellow).

It is important to mention that only agglomerates with volume > 160 µm$^3$, corresponding to a diameter of approximately 5.4 µm, were analyzed. The histogram in Figure 9 shows the volume distribution of these Ag-NPs aggregates. About 8900 of the total number of 9949 counted agglomerates are small particles with volume near the detection limit, between 160-2500 µm$^3$. Higher presence of silver aggregates with volume between 160 and 190000 µm$^3$ was observed preferentially in the parenchyma tissue.

Table 7 presents the main statistical parameters of the analyzed agglomerates. Half of the agglomerates have volume below 282 µm$^3$ (median volume). It suggests the presence of a large number of undetected small aggregates with volume below 160 µm$^3$.

Finally, the microtomography analysis showed that the aggregates are concentrated in the parenchyma tissue inside the bamboo cells. This observation is still under investigation, but it is well known that the parenchyma, a tissue with living plant cells, is open and connected to the vessels by small apertures with diameter up to 5 µm, to allow inward and outward flows of water, mineral salts and other materials useful to sustain cell life.(1,28) As shown in Figure 10, colloidal silver nanoparticles might flow through the vascular bundle into the living cell during the impregnation process.

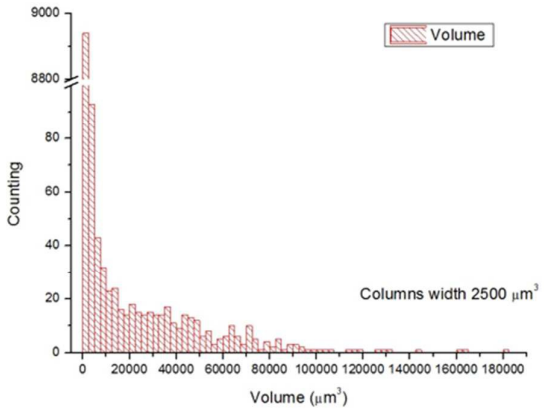


Fig. 9 Volume distribution of Ag-NPs aggregates in bamboo matrix.

Table 7 Volume statistical information of Ag-NPs aggregates population in bamboo matrix.

| **Total number of particles** | **9449** |
|---|---|
| Bamboo volume analyzed **[µm$^3$]** | 121.0x10$^9$ |
| Total Volume occupied by Ag **[µm$^3$]** | 1.86x10$^7$ |
| **Volume Ratio** | 1.54x10$^{-4}$ |
| Minimum volume of aggregate **[µm$^3$]** | 161.41 |
| Maximum volume of aggregate **[µm$^3$]** | 180057.79 |
| Median volume **[µm$^3$]** | 282.48 |
| Mean volume **[µm$^3$]** | 1967.71 |
| Standard Deviation **[µm$^3$]** | 9437.77 |

This observation supports the evidence of stronger deposition in the inner region of the parenchyma tissue. The negative charge of the citrate organic ligand, useful to stabilize the silver nanoparticles, might play an important role in the NPs distribution inside the living cells of the parenchyma tissue. In this regard other polyelectrolyte and neutral polymers capped Ag-NPs are under study to direct the silver deposition into other elements of the vascular bundle system.

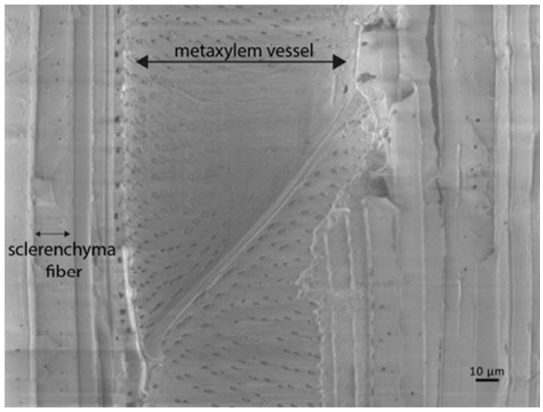


Fig. 10 SEM image of the longitudinal section of a bamboo vascular bundle shows a metaxylem vessel with a diameter of

100 µm immersed in sclerenchyma fibers and holes with diameter up to 5 µm.

**Microbiology test.** As shown in Figure 11, comparing the dry-weight fungal colonies of the control test (without NPs) with the test in presence of NPs, approximately 53% of cell dry-weight decreased in the presence of NP-01, while 47% and 7% of cell growth inhibition were obtained with CO-20 and CO-40, respectively. According to Table 5, all silver NPs used in this work presented the same concentration in the culture media (2 mg $mL^{-1}$), but their diameter and also their concentration in particles per milliliter are different. Comparing only the physical characteristics of commercial NPs, we see that lower is the diameter (d), higher is the antimicrobial effect of Ag-NPs.

In our experiments CO-20 (d=21.2nm) presented better antimicrobial effect when compared to CO-40 (d=38.9 nm) and CO-60 (d=60.3nm). Moreover, NP-01 was more efficient compared to CO-20. On the other hand, evaluating particle concentration used in this work, we observed that higher is this parameter (particle $mL^{-1}$) higher is the inhibitory effect. At the same mass element (Ag) concentration of colloids, the solution with the smallest NPs presented the highest particle concentration (NP-01, d=14.3±3.6 nm and $1.25x10^{11}$ particle $mL^{-1}$), conversely, the largest NPs diameter presented the lower particle concentration (CO-60, d=60.3±3.6 nm and $1.66x10^{9}$ particle $mL^{-1}$).

The antimicrobial tests revealed that homemade nanoparticles NP-01 in the media culture presented a particle concentration 3.3 fold higher ($1.25x10^{11}$ particle $mL^{-1}$) than the smallest commercial nanoparticle, CO-20, ($3.82x10^{10}$ particle $mL^{-1}$). So, we can state that the highest inhibition of *Aspergillus niger* growth (53% with 2.00 ppm) is due to both reasons: the smaller size diameter and the higher number of NPs able to inhibit fungus growth. None of the reference papers mentioned particle concentration (particle $mL^{-1}$) to establish the effect of silver nanoparticles on microbial cell growth. All of them compare particles size, shape and concentration of mass element (Ag) concentration (mg $mL^{-1}$ or ppm).(8,69–71) The different behavior found for CO-60 related to an increase of cell growth, compared to the control test, can be attributed to the highest particles size diameter that contributes negatively to the inhibitory effect(11,72) and to the lowest number of particles per milliliter in the media culture. Thus, the number of particles with CO-60 was not enough to inhibit properly the cell growth.

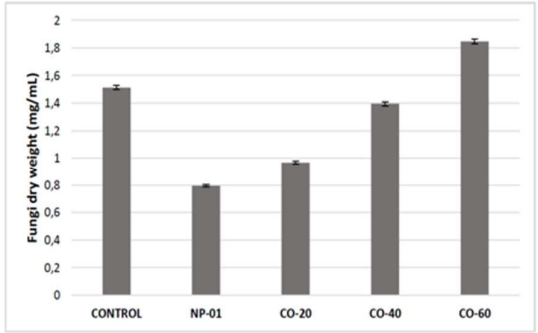


Fig. 11 Histogram of dry-weight fungal colonies after 48 hours of growth in the absence (control) and in the presence of different colloids Ag-NPs: homemade NP-01 and commercials CO-20/60.

Besides, in the absence of the inhibitory effect, citrate can be metabolized and used as additional carbon source for ATP production and additional cell growth.(73,74) It is worth mentioning that the mechanism of ATP production is the same in both bacteria and fungi. Literature reports mention that Ag-NPs effects on cells may involve different mechanisms: alteration of membrane-bound enzymes function, such as those in the respiratory chain,(73,74) loss of DNA replication ability that hinder the expression of many proteins and enzymes essential for energy production (ATP).(75,76) All these mechanisms are related to $Ag^{+}$ release from Ag-NPs directly involved in metal ion-enzymes interactions, or in tiol-binding of tiolated protein to the metal silver surface. Both can modify the protein structure and consequently its biological function.

Finally, as NP-01 was the most effective, it was used for the impregnation bamboo test specimens. Pure bamboo and engineered biocomposite Ag-NPs/bamboo were exposed to air and ambient humidity (about 70-80%) during summer time in Rio de Janeiro, Brazil. All untreated samples showed the formation of fungal colonies, while those treated with Ag-NPs were preserved and protected from the fungi degradation. The optical microscope picture in Figure 12 shows the proliferation of fungi on the bamboo surface without Ag-NPs treatment (A), while the specimen with Ag-NPs treatment (B) is free of fungal colonies.

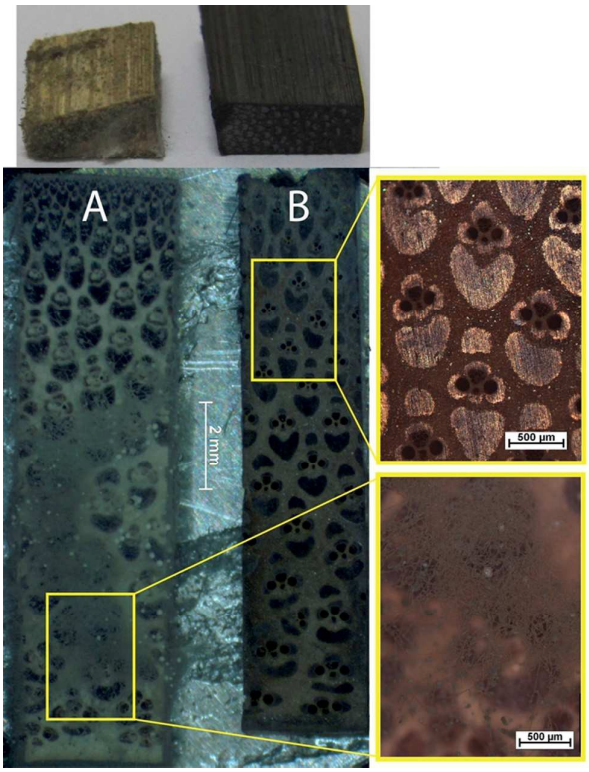


Fig. 12 Optical microscope images of bamboo specimens: (A) without Ag-NPs treatment and (B) with Ag-NPs impregnation (NP-01). On left side the natural bamboo shows

formation of fungal hyphae, while the engineered biocomposite of bamboo with Ag-NPs is free of fungi.

## Conclusions

To our best knowledge, this is the first investigation in which X-Ray microtomography analysis is used to study an engineered biocomposite metal-bamboo matrix (Ag-NP/Bamboo). Silver nanoparticles were synthesized, characterized and used to fill up bamboo specimen with the objective to protect it against fungi attack. Qualitative and quantitative analyses of Ag-NPs agglomerates population inside the bamboo matrix using 3D μCT images showed an important population of agglomerates with volumes between 160-190000 $\mu m^3$, mainly deposited on the parenchyma tissue.

From the antimicrobial tests, we state that highest inhibition of *Aspergillus niger* growth, obtained with NP-01 (53% with 2 mg $mL^{-1}$), is due to both reasons: the smaller size diameter (14.3±3.6 nm), and the higher number of NPs ($1.25x10^{11}$ particle $mL^{-1}$) able to inhibit fungus proliferation , when compared with the commercial NPs.

The results show that homemade silver colloidal solution is an effective nano-filler agent with antifungal activity able to improve the bamboo durability. The engineered biocomposite bamboo exposed to air and humidity during 5 months was free of fungal colonies, while, all untreated bamboo specimens presented a biological degradation. We believe that the use of NPs silver colloids will contribute to prevent fungal proliferation and microbiological activity for future industrial applications of engineered bamboo and wood. Our conservation method can be useful to preserve historical wooden artefact or handcraft made on bamboo.

Future studies will be focused on the selective distribution of polymer capped Ag-NPs into bamboo vascular bundles, as well as the variation of the metal volume deposition as a function of the number of impregnation cycles. Besides, the effect of different charged surfactant-capped Ag-NPs on their dispersion and their impact on bamboo degradation, will be evaluated. Pre-chemical treatments of bamboo fibers could directly interfere with adhesion of the nanoparticles and improve the impregnation of the Ag-NPs inside the biocomposite matrix.

## Acknowledgements

The authors thank CNPQ for the approval of the Project: 458302/2013-9, CAPES and FAPERJ for their financial support and the scholarship of the under graduate student (E.L.L.), master student (R.S.M.) and post-doctoral researchers (S.M.L.K. and E.C.R.). The authors thank Rafael C. C. Rocha and Jefferson R. Souza for technical assistance during ICP-MS analysis.

## Notes and references

1. Liese, Walter, Köhl M. Bamboo, The Plant and its Uses [Internet]. Liese W, Köhl M, editors. Cham: Springer International Publishing; 2015. Available from: http://link.springer.com/10.1007/978-3-319-14133-6

2. Siti S, Abdul HPS, Wan WO, Jawai M. Bamboo Based Biocomposites Material, Design and Applications. In: Materials Science - Advanced Topics [Internet]. InTech; 2013. Available from: http://www.intechopen.com/books/materials-science-advanced-topics/bamboo-based-biocomposites-material-design-and-applications

3. Gugnani HC, Paliwal-Joshi A, Rahman H, Padhye AA, Singh TSK, Das TK, et al. Occurrence of pathogenic fungi in soil of burrows of rats and of other sites in bamboo plantations in India and Nepal. Mycoses [Internet]. 2007 Nov;50(6):507–11. Available from: http://doi.wiley.com/10.1111/j.1439-0507.2007.01402.x

4. Razak Wahab MS and HWS. Fungal Colonisation and Decay in Tropical Bamboo Species. J Appliesd Sci. 2005;5(5):897–902.

5. Tanaka E. Mechanisms of bamboo witches'broom symptom devlpment caused by endophytic/epiphytic fungi. Plant Signal Behav [Internet]. 2010 Apr 31;5(4):415–8. Available from: http://www.tandfonline.com/doi/abs/10.4161/psb.5.4.10834

6. Haider A, Kang I-K. Preparation of Silver Nanoparticles and Their Industrial and Biomedical Applications: A Comprehensive Review. Adv Mater Sci Eng [Internet]. 2015;2015:1–16. Available from: http://www.hindawi.com/journals/amse/2015/165257/

7. Padovani GC, Feitosa VP, Sauro S, Tay FR, Durán G, Paula AJ, et al. Advances in Dental Materials through Nanotechnology: Facts, Perspectives and Toxicological Aspects. Trends Biotechnol [Internet]. Elsevier Ltd; 2015 Nov;33(11):621–36. Available from: http://dx.doi.org/10.1016/j.tibtech.2015.09.005

8. Kim SW, Jung JH, Lamsal K, Kim YS, Min JS, Lee YS. Antifungal Effects of Silver Nanoparticles (AgNPs) against Various Plant Pathogenic Fungi. Mycobiology [Internet]. 2012;40(1):53. Available from: http://synapse.koreamed.org/DOIx.php?id=10.5941/MYCO.2012.40.1.053

9. Kim SW, Kim KS, Lamsal K, Kim YJ, Kim S Bin, Jung M, et al. An in vitro study of the antifungal effect of silver nanoparticles on oak wilt pathogen Raffaelea sp. J Microbiol Biotechnol. 2009;19(8):760–4.

10. Mosselhy DA, El-Aziz MA, Hanna M, Ahmed MA, Husien MM, Feng Q. Comparative synthesis and antimicrobial action of silver nanoparticles and silver nitrate. J Nanoparticle Res [Internet]. 2015 Dec 9;17(12):473. Available from: http://link.springer.com/10.1007/s11051-015-3279-8

11. Agnihotri S, Mukherji S, Mukherji S. Size-controlled silver nanoparticles synthesized over the range 5–100 nm using the same protocol and their antibacterial efficacy. RSC Adv [Internet]. 2014;4(8):3974–83. Available from: http://pubs.rsc.org/en/content/articlehtml/2014/ra/c3ra4

4507k

12. Shrivastava S, Bera T, Roy A, Singh G, Ramachandrarao P, Dash D. Characterization of enhanced antibacterial effects of novel silver nanoparticles. Nanotechnology [Internet]. 2007 Jun 6;18(22):225103. Available from: http://dx.doi.org/10.1088/0957-4484/18/22/225103

13. Duncan T V. Applications of nanotechnology in food packaging and food safety: Barrier materials, antimicrobials and sensors. J Colloid Interface Sci [Internet]. 2011 Nov;363(1):1–24. Available from: http://linkinghub.elsevier.com/retrieve/pii/S0021979711008642

14. Elgorban AM, El-Samawaty AE-RM, Yassin MA, Sayed SR, Adil SF, Elhindi KM, et al. Antifungal silver nanoparticles: synthesis, characterization and biological evaluation. Biotechnol Biotechnol Equip [Internet]. 2016 Jan 2;30(1):56–62. Available from: http://www.tandfonline.com/doi/full/10.1080/13102818.2015.1106339

15. Nam G, Purushothaman B, Rangasamy S, Song JM. Investigating the versatility of multifunctional silver nanoparticles: preparation and inspection of their potential as wound treatment agents. Int Nano Lett [Internet]. Springer Berlin Heidelberg; 2016 Mar 11;6(1):51–63. Available from: http://link.springer.com/10.1007/s40089-015-0168-1

16. Zhang F, Wu X, Chen Y, Lin H. Application of silver nanoparticles to cotton fabric as an antibacterial textile finish. Fibers Polym [Internet]. 2009 Aug 27;10(4):496–501. Available from: http://link.springer.com/10.1007/s12221-009-0496-8

17. Teli MD, Sheikh J. STUDY OF GRAFTED SILVER NANOPARTICLE CONTAINING DURABLE ANTIBACTERIAL BAMBOO RAYON. Cellul Chem Technol,. 2013;47:69–75.

18. Cloutier M, Mantovani D, Rosei F. Antibacterial Coatings: Challenges, Perspectives, and Opportunities. Trends Biotechnol [Internet]. Elsevier Ltd; 2015 Nov;33(11):637–52. Available from: http://dx.doi.org/10.1016/j.tibtech.2015.09.002

19. Sarmast MK, Salehi H. Silver Nanoparticles: An Influential Element in Plant Nanobiotechnology. Mol Biotechnol [Internet]. Springer US; 2016 Jul 4;58(7):441–9. Available from: http://link.springer.com/10.1007/s12033-016-9943-0

20. Aslani F, Bagheri S, Muhd Julkapli N, Juraimi AS, Hashemi FSG, Baghdadi A. Effects of Engineered Nanomaterials on Plants Growth: An Overview. Sci World J [Internet]. 2014;2014:1–28. Available from: http://www.hindawi.com/journals/tswj/2014/641759/

21. Hamed SAM. In-vitro studies on wood degradation in soil by soft-rot fungi: Aspergillus niger and Penicillium chrysogenum. Int Biodeterior Biodegradation [Internet]. Elsevier Ltd; 2013 Mar;78:98–102. Available from: http://dx.doi.org/10.1016/j.ibiod.2012.12.013

22. Bellotti N, Romagnoli R, Quintero C, Domínguez-Wong C, Ruiz F, Deyá C. Nanoparticles as antifungal additives for indoor water borne paints. Prog Org Coatings [Internet]. Elsevier B.V.; 2015 Sep;86:33–40. Available from: http://dx.doi.org/10.1016/j.porgcoat.2015.03.006

23. Horner C.J. KA and NKR. Nanosilver as a biocie in building materials. USA; 2006. p. U.S. patent 2006/0272542 A1.

24. Hyuk-Min Kwon, Ho-Wook Yun, Shin-Chul Kang, Il-Jin Kim S-SG. Antibacterial paint containing nano silver particles. 2005. p. US 20050287112 A1.

25. El Zowalaty M, Ibrahim NA, Salama M, Shameli K, Usman M, Zainuddin N. Synthesis, characterization, and antimicrobial properties of copper nanoparticles. Int J Nanomedicine [Internet]. 2013 Nov;4467. Available from: http://www.dovepress.com/synthesis-characterization-and-antimicrobial-properties-of-copper-nano-peer-reviewed-article-IJN

26. Meghana S, Kabra P, Chakraborty S, Padmavathy N. Understanding the pathway of antibacterial activity of copper oxide nanoparticles. RSC Adv [Internet]. Royal Society of Chemistry; 2015;5(16):12293–9. Available from: http://dx.doi.org/10.1039/C4RA12163E

27. Antonio Ludovido Beraldo, Lara Durães Sette, Rodolfo Gomes MBF. Occurrence of filamentous fungi on Dendrocalamus giganteus in Brazil. In: VIII World Bamboo Congress, At Bangkpk, Thailand, Volume: 1 [Internet]. 2009. Available from: https://www.researchgate.net/publication/266260536

28. Liese W. Anatomy and properties of bamboo. Bamboo Work Hangzhou [Internet]. 1985;196–393. Available from: http://www.inbar.int/publication/PDF/INBAR_PR_03_1.pdf

29. Ghavami K, Rodrigues CS PS. Bamboo functionally graded composite material. Asian J Civ Eng. 2003;4:1–10.

30. Tan T, Rahbar N, Allameh SM, Kwofie S, Dissmore D, Ghavami K, et al. Mechanical properties of functionally graded hierarchical bamboo structures. Acta Biomater [Internet]. 2011 Oct;7(10):3796–803. Available from: http://linkinghub.elsevier.com/retrieve/pii/S1742706111002455

31. Youssefian S, Rahbar N. Molecular Origin of Strength and Stiffness in Bamboo Fibrils. Sci Rep [Internet]. Nature Publishing Group; 2015 Jun 8;5:11116. Available from: http://dx.doi.org/10.1038/srep11116

32. Ghavami K. Bamboo as reinforcement in structural concrete elements. Cem Concr Compos [Internet]. 2005 Jul;27(6):637–49. Available from: http://linkinghub.elsevier.com/retrieve/pii/S0958946504001337

33. Abdul Khalil HPS, Bhat IUH, Jawaid M, Zaidon A,

Hermawan D, Hadi YS. Bamboo fibre reinforced biocomposites: A review. Mater Des [Internet]. Elsevier Ltd; 2012 Dec;42:353–68. Available from: http://dx.doi.org/10.1016/j.matdes.2012.06.015

34. V. C. Correa, S. F. Santos, G. Marmol, A. A. S. Curvelo, H. Savastano Jr. Potential of bamboo organosolv pulp as a reinforcing element in fiber - cement materials,. Constr Build Mater. 2014;72:65–71.

35. Tiburtino RF, Paes JB, Vidaurre GB, Beraldo AL, Arantes MDC. RESISTÊNCIA DE DUAS ESPÉCIES DE BAMBU TRATADAS CONTRA FUNGOS XILÓFAGOS. Rev Árvore [Internet]. 2015 Jun;39(3):567–74. Available from: http://www.scielo.br/scielo.php?script=sci_arttext&pid=S0100-67622015000300567&lng=pt&nrm=iso&tlng=en

36. Sobrinho A, Torres SM, Barbosa NP, Ortiz SR, Ghavami K. Impregnation of Bambusa Vulgaris with Polymeric Resins. Key Eng Mater [Internet]. 2012 Jun;517:27–33. Available from: http://www.scientific.net/KEM.517.27

37. Fattah AR, Prinindya KNN, Ardhyananta H. The Effect of Chemical Substance and Immersion Time to Tensile Strength of Bamboo Betung (Dendrocalamus asper) as Chemical Preservation Treatment. IPTEK J Proc Ser [Internet]. 2014 Dec 12;1(1):1–14. Available from: http://dx.doi.org/10.12962/j23546026.y2014i1.580

38. Tang B, Sun L, Li J, Kaur J, Zhu H, Qin S, et al. Functionalization of bamboo pulp fabrics with noble metal nanoparticles. Dye Pigment [Internet]. 2015 Feb;113:289–98. Available from: http://linkinghub.elsevier.com/retrieve/pii/S0143720814003398

39. Li J, Lu Y, Wu Z, Bao Y, Xiao R, Yu H, et al. Durable, self-cleaning and superhydrophobic bamboo timber surfaces based on TiO2 films combined with fluoroalkylsilane. Ceram Int [Internet]. 2016 Jun;42(8):9621–9. Available from: http://linkinghub.elsevier.com/retrieve/pii/S0272884216301791

40. Li J, Zheng H, Sun Q, Han S, Fan B, Yao Q, et al. Fabrication of superhydrophobic bamboo timber based on an anatase TiO 2 film for acid rain protection and flame retardancy. RSC Adv [Internet]. 2015;5(76):62265–72. Available from: http://xlink.rsc.org/?DOI=C5RA09643J

41. Jin C, Li J, Han S, Wang J, Yao Q, Sun Q. Silver mirror reaction as an approach to construct a durable, robust superhydrophobic surface of bamboo timber with high conductivity. J Alloys Compd [Internet]. Elsevier B.V.; 2015 Jun;635:300–6. Available from: http://dx.doi.org/10.1016/j.jallcom.2015.02.047

42. Li J, Wu Z, Bao Y, Chen Y, Huang C, Li N, et al. Wet chemical synthesis of ZnO nanocoating on the surface of bamboo timber with improved mould-resistance. J Saudi Chem Soc [Internet]. King Saud University; 2016 Jan; Available from: www.ksu.edu.sa

43. Yu Y, Jiang Z, Wang G, Tian G, Wang H, Song Y. Surface functionalization of bamboo with nanostructured ZnO. Wood Sci Technol [Internet]. 2012 Jul 18;46(4):781–90. Available from: http://link.springer.com/10.1007/s00226-011-0446-7

44. Pandoli O, Ventura Pereira-Meirelles F, Monteiro Lobo Lobo Luz E, Assumpção A, dos Santos Martins R, del Rosso T, et al. Synthesis of Silver Nanoparticles with Potential Antifungical Activity for Bamboo Treatment. Key Eng Mater [Internet]. 2015 Oct;668:86–91. Available from: http://www.scientific.net/KEM.668.86

45. CAVALIER-SMITH T. A revised six-kingdom system of life. Biol Rev [Internet]. 2007 Jan 11;73(3):203–66. Available from: http://doi.wiley.com/10.1111/j.1469-185X.1998.tb00030.x

46. Ka P, Es D, Mjg V. Endophytic fungi associated with bamboo as possible sources of single cell protein using corn cob as a substrate. Micosphere. 2016;7(February):139–47.

47. Walisko R, Krull R, Schrader J, Wittmann C. Microparticle based morphology engineering of filamentous microorganisms for industrial bio-production. Biotechnol Lett [Internet]. 2012 Nov 11;34(11):1975–82. Available from: http://link.springer.com/10.1007/s10529-012-0997-1

48. E. S, N. D-C, J. F, Dijck P van. On the safety of Aspergillus niger - a review. Appl Microbiol Biotechnol [Internet]. 2002 Jan 1;59(4–5):426–35. Available from: http://link.springer.com/10.1007/s00253-002-1032-6

49. Dashtban M, Schraft H, Syed TA, Qin W. Fungal biodegradation and enzymatic modification of lignin. Int J Biochem Mol Biol [Internet]. 2010;1(1):36–50. Available from: http://www.ncbi.nlm.nih.gov/pubmed/21968746

50. Fuentes CA, Tran LQN, Dupont-Gillain C, Vanderlinden W, De Feyter S, Van Vuure AW, et al. Wetting behaviour and surface properties of technical bamboo fibres. Colloids Surfaces A Physicochem Eng Asp [Internet]. Elsevier B.V.; 2011 May;380(1–3):89–99. Available from: http://dx.doi.org/10.1016/j.colsurfa.2011.02.032

51. Cnudde V, Boone MN. High-resolution X-ray computed tomography in geosciences: A review of the current technology and applications. Earth-Science Rev [Internet]. 2013 Aug;123:1–17. Available from: http://linkinghub.elsevier.com/retrieve/pii/S001282521300069X

52. Francis Kumi, Mao Hanping, Hu Jianping IU. Review of applying X-ray computed tomography for imaging soil-root physical and biological processes. Int J Agric Biol Eng. 2015;8:1–14.

53. S. Paciornik MHPM. Digital imaging in: G. F. V. Voort, ASM Handbook Vol. 9 Metallography and Microstructures, ASM International, Ohio,. 2004.

54. Alves H, Lima I, Assis JT, Geraldes M, Lopes RT. Comparison of pore space features by thin sections and X-ray microtomography. Appl Radiat Isot [Internet]. 2014 Dec;94:182–90. Available from: http://linkinghub.elsevier.com/retrieve/pii/S0969804314003042

55. De-Deus G, Marins J, de Almeida Neves A, Reis C, Fidel S, Versiani MA, et al. Assessing Accumulated Hard-tissue Debris Using Micro–computed Tomography and Free Software for Image Processing and Analysis. J Endod [Internet]. 2014 Feb;40(2):271–6. Available from: http://linkinghub.elsevier.com/retrieve/pii/S0099239913006468

56. De-Deus G, Silva EJNL, Marins J, Souza E, Neves A de A, Gonçalves Belladonna F, et al. Lack of Causal Relationship between Dentinal Microcracks and Root Canal Preparation with Reciprocation Systems. J Endod [Internet]. 2014 Sep;40(9):1447–50. Available from: http://linkinghub.elsevier.com/retrieve/pii/S0099239914001952

57. Ketcham RA, Carlson WD. Acquisition, optimization and interpretation of X-ray computed tomographic imagery: applications to the geosciences. Comput Geosci [Internet]. 2001 May;27(4):381–400. Available from: http://linkinghub.elsevier.com/retrieve/pii/S0098300400001163

58. Lima I, Appoloni C, Oliveira L De, Lopes T. Caracterização De Materiais Cerâmicos Através Da Microtomografia Computadorizada 3D. Rev Bras Arqueometria Restauração Conserv. 2007;1(2):22–7.

59. Long H, Swennen R, Foubert A, Dierick M, Jacobs P. 3D quantification of mineral components and porosity distribution in Westphalian C sandstone by microfocus X-ray computed tomography. Sediment Geol [Internet]. 2009 Sep;220(1–2):116–25. Available from: http://linkinghub.elsevier.com/retrieve/pii/S0037073809001626

60. Machado a. HL, Pandoli O, Miranda LSM, de Souza ROM a. Microreactors: New Opportunities in Chemical Synthesis. Rev Virtual Química [Internet]. 2014;6(4):1076–85. Available from: http://www.gnresearch.org/doi/10.5935/1984-6835.20140068

61. Haimon Diniz Lopes Alves. 3D digital video rendered from the µCT reconstructed images [Internet]. Available from: https://www.youtube.com/watch?v=gbbyCVz3Pw0g

62. Schindelin J, Arganda-Carreras I, Frise E, Kaynig V, Longair M, Pietzsch T, et al. Fiji: an open-source platform for biological-image analysis. Nat Methods [Internet]. 2012 Jun 28;9(7):676–82. Available from: http://www.nature.com/doifinder/10.1038/nmeth.2019

63. Eliceiri KW, Berthold MR, Goldberg IG, Ibáñez L, Manjunath BS, Martone ME, et al. Biological imaging software tools. Nat Methods [Internet]. 2012 Jun 28;9(7):697–710. Available from: http://www.ncbi.nlm.nih.gov/pubmed/22743775

64. Desai R, Mankad V, Gupta SK, Jha PK. Size Distribution of Silver Nanoparticles: UV-Visible Spectroscopic Assessment. Nanosci Nanotechnol Lett [Internet]. 2012 Jan 1;4(1):30–4. Available from: http://openurl.ingenta.com/content/xref?genre=article&issn=1941-4900&volume=4&issue=1&spage=30

65. Bhattacharjee S. DLS and zeta potential - What they are and what they are not? J Control Release [Internet]. Elsevier B.V.; 2016 Aug;235:337–51. Available from: http://dx.doi.org/10.1016/j.jconrel.2016.06.017

66. Zhang Y, Wang F, Yin H, Hong M. Nonuniform Distribution of Capping Ligands Promoting Aggregation of Silver Nanoparticles for Use as a Substrate for SERS. 2013;2013(May):104–11.

67. Bell SEJ, Sirimuthu NMS. Surface-Enhanced Raman Spectroscopy as a Probe of Competitive Binding by Anions to Citrate-Reduced Silver Colloids. 2005;7405–10.

68. Munro CH, Smith WE, Garner M, Clarkson J, White PC. Characterization of the Surface of a Citrate-Reduced Colloid Optimized for Use as a Substrate for Surface-Enhanced Resonance Raman Scattering. Langmuir. 1995;11(26):3712–20.

69. Pulit J, Banach M, Szczygłowska R, Bryk M. Nanosilver against fungi. Silver nanoparticles as an effective biocidal factor. Acta Biochim Pol. 2013;60(4):795–8.

70. Agnihotri S, Mukherji S, Mukherji S. Size-controlled silver nanoparticles synthesized over the range 5–100 nm using the same protocol and their antibacterial efficacy. RSC Adv [Internet]. 2014;4(8):3974–83. Available from: http://pubs.rsc.org/en/content/articlehtml/2014/ra/c3ra44507k

71. Kasprowicz MJ, Kozioł M, Gorczyca A. The effect of silver nanoparticles on phytopathogenic spores of Fusarium culmorum. Can J Microbiol. 2010;56(March):247–53.

72. Raza M, Kanwal Z, Rauf A, Sabri A, Riaz S, Naseem S. Size- and Shape-Dependent Antibacterial Studies of Silver Nanoparticles Synthesized by Wet Chemical Routes. Nanomaterials [Internet]. 2016;6(4):74. Available from: http://www.mdpi.com/2079-4991/6/4/74

73. McDonnell G, Russell AD. Antiseptics and disinfectants: activity, action, and resistance. Clin Microbiol Rev [Internet]. 1999 Jan;12(1):147–79. Available from: http://www.ncbi.nlm.nih.gov/pubmed/9880479

74. Bragg PD, Rainnie DJ. The effect of silver ions on the respiratory chain of Escherichia coli. Can J Microbiol [Internet]. 1974 Jun;20(6):883–9. Available from: http://www.ncbi.nlm.nih.gov/pubmed/4151872

75. Feng QL, Wu J, Chen GQ, Cui FZ, Kim TN, Kim JO. A mechanistic study of the antibacterial effect of silver ions

on Escherichia coli and Staphylococcus aureus. J Biomed Mater Res [Internet]. 2000 Dec 15;52(4):662–8. Available from: http://www.ncbi.nlm.nih.gov/pubmed/11033548

76. Yamanaka M, Hara K, Kudo J. Bactericidal actions of a silver ion solution on Escherichia coli, studied by energy-filtering transmission electron microscopy and proteomic analysis. Appl Environ Microbiol [Internet]. 2005 Nov;71(11):7589–93. Available from: http://www.ncbi.nlm.nih.gov/pubmed/16269810

99x35mm (300 x 300 DPI)